

# Projected Belief Networks With Discriminative Alignment for Acoustic Event Classification: Rivaling State of the Art CNNs

Paul M. Baggenstoss Fraunhofer FKIE, Fraunhoferstrasse 20

53343 Wachtberg, Germany

Email: p.m.baggenstoss@ieee.org

Kevin Wilkinghoff Fraunhofer FKIE

Email: kevin.wilkinghoff@ieee.org

Felix Govaers Fraunhofer FKIE

Email: felix.govaers@fkie.fraunhofer.de

Frank Kurth Fraunhofer FKIE

Email: frank.kurth@fkie.fraunhofer.de

**Index Terms**—Bayesian classifier, generative model, PDF estimation, projected belief network, acoustic event classification

**Abstract**—The projected belief network (PBN) is a generative stochastic network with tractable likelihood function based on a feed-forward neural network (FFNN). The generative function operates by “backing up” through the FFNN. The PBN is two networks in one, a FFNN that operates in the forward direction, and a generative network that operates in the backward direction. Both networks co-exist based on the same parameter set, have their own cost functions, and can be separately or jointly trained. The PBN therefore has the potential to possess the best qualities of both discriminative and generative classifiers. To realize this potential, a separate PBN is trained on each class, maximizing the generative likelihood function for the given class, while minimizing the discriminative cost for the FFNN against “all other classes”. This technique, called *discriminative alignment* (PBN-DA), aligns the contours of the likelihood function to the decision boundaries and attains vastly improved classification performance, rivaling that of state of the art discriminative networks. The method may be further improved using a hidden Markov model (HMM) as a component of the PBN, called PBN-DA-HMM. This paper provides a comprehensive treatment of PBN, PBN-DA, and PBN-DA-HMM. In addition, the results of two new classification experiments are provided. The first experiment uses air-acoustic events, and the second uses underwater acoustic data consisting of marine mammal calls. In both experiments, PBN-DA-HMM attains comparable or better performance as a state of the art CNN, and attains a factor of two error reduction when combined with the CNN.

## I. INTRODUCTION

### A. Generative vs. Discriminative Classification

Classification is probably the most important task in machine learning because it involves making decisions between several possible ways to understand the data. Until the advent of deep learning, this task was best solved by the human mind in conjunction with human senses and perception. There

remain two distinct approaches to classification: the generative approach, and the discriminative approach [1], [2]. Both approaches find parallels in human perception and decision-making.

In the generative approach, an attempt is made to characterize each class individually by estimating a set of patterns or parameters, then later compare the data to each stored characterization. In statistical terms, the probability distribution of the data is estimated for each class hypothesis, and later the *likelihood* of the data is determined with respect to each learned distribution estimate. In human perception, the generative approach corresponds to recognizing something based on our memory of what the class should look or sound like.

In the discriminative approach, an attempt is made to distinguish between the existing class hypotheses, an approach that is inherently more efficient and generally provides performance superior to the generative approach [2]. In human perception, the discriminative approach corresponds to looking or listening for characteristic clues that can distinguish between hypotheses. For example, if we know that two identical twins differ only in a birthmark, we look for the presence of this hard-to see characteristic.

The generative approach is inherently inefficient because it is *blind* to the other class hypotheses, so does not know in advance which subtle clues it needs, and must extract a complete detailed characterization of each class hypothesis. As the data dimension increases, the amount of information required to adequately characterize the data distribution rises exponentially, outstripping what is available in the training data. This is the so-called curse of dimensionality [2]. The generative approach becomes even more difficult in noisy scenarios because generative models cannot distinguish between the target signal and noise.

Despite these problems, generative classifiers are very useful, especially in open-set classification problems where they

This work was supported jointly by the Office of Naval Research Global and the Defense Advanced Research Projects Agency under Research Grant - N62909-21-1-2024

can detect out-of-set events. In addition, having a “second opinion” from a generative approach can result in improved performance for a combined generative/discriminative approach.

### B. Attaining the best properties of both approaches

When combining classifiers, such as by additively combining the classifier statistics (i.e. ensembling), it is important that the two methods (a) have comparable performance and (b) are based on independent views of the data. This is why it is important to create better-performing generative classifiers to combine with purely discriminative ones. Therefore, it would be desirable if generative classifiers could be constructed to utilize discriminative information, analogous to how humans do, and thereby achieve improved performance. Later, in the experiments, we will combine PBN with a discriminative CNN, but this is not what we mean by a combined approach. This is because the two methods are not able to benefit from each other during training. Using PBN, it is possible to apply both the generative and discriminative approaches simultaneously, that is to create a generative model with discriminative capability. Even if this approach does not improve upon state of the art discriminative classifiers, it could result in a classifier that is better for combination with them.

In human perception, we use a combined generative and discriminative approach if we give discriminative clues priority as we collect clues for the generative approach. To use the example of the identical twins above, we would add the presence of a birthmark to the list of features that describe each class individually. So, conceptually, a combined approach is not hard to understand. Does there exist a parallel idea in machine learning, in which a given feature extractor (i.e. a given network) can be both generative and discriminative?

Many methods have been proposed that either incorporate both generative and discriminative ideas or achieve the goal of joint generative and discriminative training [3], [4], [5], [6], [7], [8]. But these approaches concentrate on training methods, and do not treat the problem at the fundamental level that we are proposing.

### C. Discriminative and Generative functions in a single network

To have both discriminative and generative functions in a single network, the network needs to operate in both the forward and backward directions. We will call this a two-directional network, so as not to confuse the idea with bi-directional networks<sup>1</sup> [9] because it can operate in the forward direction (i.e. as a feed-forward classifier network), but also in the backward direction (as a generative network), using the same network architecture and parameter set. We seek the following properties of a two-directional network:

- 1) The desired network topology must be dimension-reducing in order to serve also as a classifier.
- 2) The generative function should be complete, which means it should provide a tractable likelihood function

(LF) (i.e. log of the probability density function) of the input data, and should be able to synthesize samples corresponding to this LF.

- 3) To be a truly dimension-reducing two-directional network, we propose that the reverse path should constitute a *right inverse* operation. If the forward path is written  $\mathbf{z} = T(\mathbf{x})$ , where  $\mathbf{x} \in \mathbb{R}^N$ ,  $\mathbf{z} \in \mathbb{R}^M$ ,  $N > M$ , and the right inverse is written  $\mathbf{x} = T^{-1}(\mathbf{z})$ , then we must have  $T(T^{-1}(\mathbf{z})) = \mathbf{z}$ . This is important because or stated goal is that the discriminative (forward path) and generative (backward path) should learn jointly. The right-inverse property insures a tight connection between the two directions. In fact, it should be clear that the right-inverse property can only be achieved by a single network, i.e. not by separate networks that each operate in one direction, because the reverse path is the inverse of the forward path.

There are a number of existing machine learning approaches that we can consider.

Although they are not right-inverse networks, we discuss two related approaches: auto-encoders and stacked restricted Boltzmann machines (RBMs). The RBM consists of two back-to-back stochastic perceptron layers with tied weights (the backward weight matrix is the transpose of the forward weight matrix) [10]. Although the reverse path of the RBM is not a right inverse, it uses the same weight matrix and is a generative network based on an elegant theory, so is worth looking at. The input data (visible data) and the hidden variables are jointly distributed according to the Gibbs distribution. The RBM is trained using an approximate maximum likelihood approach called contrastive divergence (CD) [11]. Once trained, either direction of the RBM can be converted into a perceptron layer by replacing the stochastic perceptrons with deterministic activation functions equal to their expected value. Multiple deterministic RBM perceptron layers can then be cascaded together (in both directions) to obtain a stacked RBM. The stacked RBM has also a statistical interpretation and can be trained by a multi-layer version of CD called up-down algorithm [10].

A stacked RBM is a multi-layer two-directional network without right-inverse, and is identical to an auto-encoder with tied analysis and synthesis weights, but trained differently. Note that it is not uncommon to tie the analysis and synthesis weight matrices of an auto-encoder (i.e. so that their corresponding linear operations are transposed versions of each other), which is possible both for dense and convolutional layers [12]. Auto-encoders are in wide-spread use because it is inherently useful to find a low-dimensional output feature set (called the encoding or *bottleneck* features) with minimum dimension that can be used to reconstruct the input data.

In addition to lacking a right-inverse, these networks are also not complete generative models, because they lack a tractable LF. Even the stacked RBM, which has a well-defined statistical model [10], cannot be tractably marginalized to obtain the likelihood function of the input data. A variational auto-encoder (VAE) is a type of auto-encoder [13], [14], [15], but the LF must be approximated and it is not a right-inverse network.

<sup>1</sup>Bi-directional networks have some layers that operate forward in time and some layers that operate backward in time.

Normalizing flows (NF) [16] provide a way of defining a probability distribution by finding a 1:1 dimension-preserving transformation that maps the input data to a well-defined distribution such as to independent identically-distributed (*iid*) uniform or normal random variables. The distribution of the input data is found using the change of variables theorem, i.e. using the determinant of the transformation's Jacobian matrix. The forward path extracts the *iid* random variables, and the reverse path creates synthetic input data. The problem with NF is that the forward path is not dimension-reducing, so cannot be used as a discriminative classifier. That is unfortunate because NF is truly two-directional and has a well-defined likelihood function. In order to get around the requirement of dimension-preserving transformations, a way to combine NF with variational autoencoders (VAEs) called "SurVAE" has been proposed, [17]. However, for the case of dimension-reducing deterministic transformations (surjections), SurVAE is the same as and is a re-invention of PDF projection [18], which is the basis of our proposed approach and will be reviewed in the next section.

#### D. What's New in This Paper

The approaches presented in this paper can all be found in various forms in existing conference and journal publications [19], [20], [21], [22], [23], [24], [25], [26], [27], [28], [29]. However, there is no comprehensive and cohesive treatment to make the idea set accessible to readers. This paper seeks to fill this void. The experimental results are also new, as well as the way the concepts are introduced, specifically in the context of a two-directional network.

## II. REVIEW OF PDF PROJECTION

### A. Definition of PDF Projection

Before we introduce the projected belief network (PBN), we need to introduce and review PDF projection, the principle upon which it is based. Consider a fixed and differentiable dimension-reducing transformation  $\mathbf{z} = T(\mathbf{x})$ , where  $\mathbf{x} \in \mathbb{X} \subseteq \mathbb{R}^N$ , and  $\mathbf{z} \in \mathbb{R}^M$ , where  $M < N$ , and whose  $N \times M$  matrix of partial derivatives is of full rank. Then, assuming a known or assumed feature distribution  $g(\mathbf{z})$ , one can construct a probability density function (PDF) on the input data with support  $\mathbb{X}$  given by

$$G(\mathbf{x}) = \frac{p_{0,x}(\mathbf{x})}{p_{0,x}(\mathbf{z})} g(\mathbf{z}), \quad (1)$$

where  $p_{0,x}(\mathbf{x})$  is a prior distribution with support on  $\mathbb{X}$  and  $p_{0,x}(\mathbf{z})$  is its mapping to  $\mathbb{R}^M$  through  $T(\mathbf{x})$ . In our simplified notation, the argument of the distribution defines its range of support, and the variable in the subscript defines the original range where the distribution was defined. Therefore,  $p_{0,x}(\mathbf{z})$  is a distribution over the range of  $\mathbf{z}$ , but is a mapping of a distribution that was defined on  $\mathbb{X}$ . Note that  $G(\mathbf{x})$  is seen as a function only of  $\mathbf{x}$  since  $\mathbf{z}$  is deterministically determined from  $\mathbf{x}$  using  $\mathbf{z} = T(\mathbf{x})$ . In fact, it can be shown [19], [21] that  $G(\mathbf{x})$  is a PDF (integrates to 1) and is a member of the set of PDFs that map to  $g(\mathbf{z})$  through  $T(\mathbf{x})$ . If  $p_{0,x}(\mathbf{x})$  is selected for maximum entropy, then  $G(\mathbf{x})$  is unique for a given

transformation, data range  $\mathbb{X}$ , and a given  $g(\mathbf{z})$  (where "g" represents the "given" feature distribution). One can think of  $G(\mathbf{x})$  as a constructed distribution based on a set of parameters (i.e. the parameters of  $T(\mathbf{x})$ , which could be a neural network for example). Then, using the method of maximum likelihood, the PDF of the input data can be estimated by training the parameters of the transformation to maximize the mean of  $\log G(\mathbf{x})$  over a set of training data. This in fact results in a transformation that extracts sufficient statistics and maximizes information [22] (see Section II-E). We say that  $G(\mathbf{x})$  is the "projection" of  $g(\mathbf{z})$  back to the input data range  $\mathbb{X}$ , i.e. a *back-projection*. We call the term  $J(\mathbf{x}) \triangleq \frac{p_{0,x}(\mathbf{x})}{p_{0,x}(\mathbf{z})}$  the "J-function" because in the special case of dimension-preserving transformations (i.e. normalizing flows [16]),  $J(\mathbf{x})$  is the determinant of the Jacobian of  $T(\mathbf{x})$ . The log of the J-function is analogous to the "likelihood contribution" found in [17].

### B. Data Generation

To generate data from  $G(\mathbf{x})$  in (1), one draws a sample  $\mathbf{z}$  from  $g(\mathbf{z})$ , then draws a sample  $\mathbf{x}$  from the level set  $\mathcal{L}(\mathbf{z})$  defined by

$$\mathcal{L}(\mathbf{z}) = \{\mathbf{x} \in \mathbb{X} | T(\mathbf{x}) = \mathbf{z}\}, \quad (2)$$

and weighted by the prior distribution  $p_{0,x}(\mathbf{x})$ . In other words, we sample from  $p_{0,x}(\mathbf{x})$  restricted and normalized on  $\mathcal{L}(\mathbf{z})$ .

Depending on the transformation  $T$  and prior distribution  $p_{0,x}(\mathbf{x})$ , sampling may be straight forward, or may require Markov Chain Monte Carlo (MCMC) methods. PDF projection sampling for specific examples of transformations are treated in [21], [23].

### C. Chain Rule

In order to implement (1), it is necessary to know  $p_{0,x}(\mathbf{z})$ . For complex non-linear transformations, it may be impossible to find a tractable form for  $p_{0,x}(\mathbf{z})$ . However, using the chain-rule, it is possible to solve the problem by breaking the transformation into a cascade of simpler transformations and applying the PDF projection idea recursively to stages of a transformation. Consider a cascade of two transformations,  $\mathbf{y} = T_1(\mathbf{x})$ , and  $\mathbf{z} = T_2(\mathbf{y})$ . Then, applying (1) recursively,

$$G(\mathbf{x}) = \frac{p_{0,x}(\mathbf{x})}{p_{0,x}(\mathbf{y})} \frac{p_{0,y}(\mathbf{y})}{p_{0,y}(\mathbf{z})} g(\mathbf{z}), \quad (3)$$

which can be extended to any number of stages. To compute  $\log G(\mathbf{x})$ , one just accumulates the log-J function of the transformations. Data generation is also cascaded, and is initiated by drawing a sample  $\mathbf{z}$  from  $g(\mathbf{z})$ .

### D. Multiple features

In recent years, end-to-end deep learning approaches are slowly making feature extraction obsolete. But, generative classification approaches are rarely used on unprocessed data. Some form of feature extraction, such as conversion to time-frequency spectral features, is carried out before application of generative models because this tends to reduce dimensionality and remove nuisance information such as phase. However, data



can sometimes have very diverse character and just one feature extraction approach may not suffice.

But, the problem with using multiple feature extraction approaches in generative models is that the definition of “input data” is not clear when there are several feature sets. This problem is solved by PDF projection because all feature extraction transformations can project back to the same input data space.

There are a number of approaches to using PDF projection for this purpose. One possible approach is to assign an individually optimized feature set to each data class. But, using one feature extraction for *each* data class can be problematic. For example, the existence of background noise in the data could make a different feature extractor more “suitable”, increasing the likelihood values for that feature/class combination and cause classification errors. Therefore, it is safer and more effective to use the same set of feature extraction approaches for all classes. Using PDF projection, the likelihood function computed for each feature after back-projecting to the raw data can be seen as a component of a mixture distribution [24], [25]. This brings much more information to bear on the problem without increasing the dimensionality of the generative models.

To add mathematical detail, consider  $L$  feature extraction chains, resulting in features  $\mathbf{z}_1, \dots, \mathbf{z}_L$ , with feature probability density functions  $g_1(\mathbf{z}_1), \dots, g_L(\mathbf{z}_L)$ . Applying (1) separately to each model, we arrive at the projected PDFs  $G_1(\mathbf{x}), \dots, G_L(\mathbf{x})$ . The mixture distribution can be created as follows

$$G(\mathbf{x}) = \sum_{i=1}^L \alpha_i G_i(\mathbf{x}).$$

Such a mixture model is then trained separately on each class, with the weights  $\{\alpha_i\}$  also considered as parameters to estimate.

However, a problem that arises when using multiple feature sets is caused by the widely-used technique of overlapped, windowed segmentation of time-series. While it is reasonable to compare likelihood values for features extracted from the same input data, it is not clear about how to resolve the differences between two feature extractors operating on essentially different raw data. When applying different overlapped segmentation prior to feature extraction, the definition of “raw data” changes with the segmentation window-size. A solution to this problem is provided by what we call Hanning-3 segmentation, [30], however this is out of scope for this paper.

#### E. Information Maximization by PDF Projection

Dimension-reduction is an important function in neural networks and machine learning with many end-goals including classification, auto-encoding, and feature embedding. When the end-goal is not known in advance, one can try to maximize the information at the output. A widely-used criteria for maximizing information transfer is the InfoMax principle, which seeks to maximize the mutual information (MI) between the input data  $\mathbf{x}$  and output data  $\mathbf{z}$  [31], [32], [33], [34]. The mutual information can be decomposed as

$$I(\mathbf{x}, \mathbf{z}) = H(\mathbf{z}) - H(\mathbf{z}|\mathbf{x}),$$

where  $H(\mathbf{z})$  and  $H(\mathbf{z}|\mathbf{x})$  are the entropy and conditional entropy [32], [35]. For noiseless deterministic transformations,  $\mathbf{z}$  is known perfectly given  $\mathbf{x}$ , so  $H(\mathbf{z}|\mathbf{x}) = 0$  [32], [35]. Thus, the task comes down to maximizing the entropy of the network output  $\mathbf{z}$  [32]. But this is not very satisfactory as an information metric because  $H(\mathbf{z})$  can be made as large as possible simply by scaling or applying 1:1 transformations which do not change the information content. To arrive at meaningful results with InfoMax, one has to impose an arbitrary constraint, such as variance or data range. A more satisfactory criterion was proposed in [22]. The proposed approach is to quantify the separability of the input data distribution  $p(\mathbf{x})$  from a maximum entropy (MaxEnt) reference distribution  $p_0(\mathbf{x})$  through the Kullback-Leibler divergence (KLD), written  $D(p||p_0)$ , where  $D(p||q)$  is the KLD :

$$D(p||q) \triangleq \mathbb{E}_p \left\{ \log \frac{p(\mathbf{x})}{q(\mathbf{x})} \right\}. \quad (4)$$

A MaxEnt distribution  $p_0(\mathbf{x})$  is bland and featureless, so it makes sense that the data distribution  $p(\mathbf{x})$  stands out relative to it. The idea is that for maximum information flow, the separability of the two distributions should not be reduced by the network, or in other words, we try to maximize the divergence at the output, which is bounded by the divergence at the input. It is shown in [22], that this same goal is achieved by PDF projection when one estimates the distribution the input data by fitting  $G(\mathbf{x})$  to  $p(\mathbf{x})$  using maximum likelihood and the available training data:

$$\max_T \left\{ \sum_i \log G(\mathbf{x}_i; T, g) \right\}, \quad (5)$$

where we have added  $T$  and  $g$  as arguments to  $G(\mathbf{x})$  to make clear that (1) depends on transformation  $T$  and given feature density  $g$ . It is interesting to note that as (5) is maximized over  $T$ , the true feature distribution is in fact driven toward  $g(\mathbf{z})$ . A side-benefit of this is that if  $g(\mathbf{z})$  is some canonical distribution of (*iid*) output variables, then the true feature distribution is driven toward  $g(\mathbf{z})$ , i.e.  $p(\mathbf{z}) \rightarrow g(\mathbf{z})$ . Therefore, (5) achieves three goals at the same time :

- 1) Maximization of information flow.
- 2) PDF estimation, i.e.  $G(\mathbf{x}_i; T, g) \rightarrow p(\mathbf{x})$ .
- 3) Generation of information-bearing statistics  $\mathbf{z}$  with arbitrary desired distribution as  $p(\mathbf{z}) \rightarrow g(\mathbf{z})$ .

### III. PROJECTED BELIEF NETWORK (PBN)

#### A. Definition of PBN

When PDF projection is applied to a feed-forward neural network (FFNN) layer-by-layer, this results in the projected belief network (PBN) [36]. The PBN is a true two-directional network because the reverse path (sampling) is carried out backwards through the FFNN and is a right-inverse.

#### B. Mathematical Details of a PBN Layer

We concentrate on a single PBN layer, which corresponds to one perceptron layer in a neural network. To illustrate the sampling process in one layer, let  $\mathbf{y} \in \mathbb{R}^M$  be the

TABLE I

MAXENT PRIORS AND ACTIVATION FUNCTIONS AS A FUNCTION OF INPUT DATA RANGE. TG="TRUNC. GAUSS.". TED="TRUNC. EXPON. DISTR".

$$\mathcal{N}(x) \triangleq \frac{e^{-x^2/2}}{\sqrt{2\pi}} \text{ AND } \Phi(x) \triangleq \int_{u=-\infty}^x \mathcal{N}(u) du.$$

$\mathbb{X}$	MaxEnt Prior		Activation	
	$p_{0,x}(\mathbf{x})$	Name	$\lambda(\alpha)$	Name
$\mathbb{R}^N$	$\prod_{i=1}^N \mathcal{N}(x_i)$	Gaussian	$\alpha$	linear
$\mathbb{P}^N$	$\prod_{i=1}^N 2\mathcal{N}(x_i)$	Trunc. Gauss.	$\alpha + \frac{\mathcal{N}(\alpha)}{\Phi(\alpha)}$	TG
$\mathbb{P}^N$	$\prod_{i=1}^N \frac{1}{2} e^{-x_i/2}$	Expon.	$\frac{2}{1-2\alpha}, \alpha < .5$	Expon.
$\mathbb{U}^N$	1	Uniform	$\frac{e^\alpha}{e^\alpha - 1} - \frac{1}{\alpha}$	TED

hidden variable at the output of a given layer of a FFNN, and let  $\mathbf{x} \in \mathbb{R}^N$  be the layer input, where  $N > M$ . Let  $\mathbf{y} = \lambda(\mathbf{b} + \mathbf{W}'\mathbf{x})$ , where  $\mathbf{W}, \mathbf{b}$  are the layer weight matrix and bias, and  $\lambda(\cdot)$  is a strictly monotonic increasing (SMI) element-wise activation function. We seek to sample  $\mathbf{x}$  given  $\mathbf{y}$ . Because the SMI activation function and bias are invertible, it is equivalent to sample  $\mathbf{x}$  given  $\mathbf{z}$ , where  $\mathbf{z} = \mathbf{W}'\mathbf{x}$ . This is done by drawing  $\mathbf{x}$  randomly from the set of samples that map to  $\mathbf{z}$ , weighted by prior distribution  $p_{0,x}(\mathbf{x})$ . More precisely,  $\mathbf{x}$  is drawn from level set (2), which in the case of a linear transformation is the set (an affine subset and a manifold)

$$\mathcal{M}(\mathbf{z}) = \{\mathbf{x} \in \mathbb{X} | \mathbf{W}'\mathbf{x} = \mathbf{z}\}, \quad (6)$$

with prior density  $p_{0,x}(\mathbf{x})$ . This prior is selected according to the principle of maximum entropy (MaxEnt) [37], so it has the highest possible entropy subject to any constraints. These constraints include the range of the variable  $\mathbf{x}$ , denoted by  $\mathbb{X}$ , determined by which activation function was used in the up-stream layer, and some moment constraints that may be necessary when  $\mathbb{X}$  is unbounded. By definition, the drawn sample will be a right-inverse (i.e. preimage) of  $\mathbf{z}$ .

Note that when discussing PBNs, we use the variable  $\mathbf{x}$  to denote either a layer input or a network input, depending on the context. The variable  $\mathbf{z}$  always refers to the output of the linear transformation, and the variable  $\mathbf{y}$  always refers to the output of an activation function,

We consider three canonical data ranges that are common in machine learning,  $\mathbb{R}^N : x_i \in (-\infty, \infty), \forall i$ ,  $\mathbb{P}^N : x_i \in [0, \infty), \forall i$ , and  $\mathbb{U}^N : x_i \in [0, 1], \forall i$ . In Table I, we list four useful combinations of data range  $\mathbb{X}$  and MaxEnt prior  $p_{0,x}(\mathbf{x})$ . Note that when a data range is defined that is unbounded, the entropy of a distribution with support on that range can go to infinity. Therefore, to find a MaxEnt distribution, it is necessary to place constraints on the moments, either variance or mean. This is why the MaxEnt distributions are defined either with a fixed variance (Gaussian or truncated Gaussian) or fixed mean (exponential). Additional details can be found in [26], [27].

The PDF of the input data of a PBN layer is given by the projected PDF (1), which can be seen as an application of Bayes rule [21]  $G(\mathbf{x}) = p_m(\mathbf{x}|\mathbf{z})g(\mathbf{z})$ , where  $p_m(\mathbf{x}|\mathbf{z})$  is the *a posteriori* distribution, also equal to the J-function, i.e.

$$p_m(\mathbf{x}|\mathbf{z}) = \frac{p_{0,x}(\mathbf{x})}{p_{0,x}(\mathbf{z})} = J(\mathbf{x}). \quad (7)$$

Note that  $p_m(\mathbf{x}|\mathbf{z})$  is a manifold distribution with support only on a set of zero volume, the manifold (6). To see this, we integrate the J-function on the manifold for fixed  $\mathbf{z}$ :

$$\int_{\mathbf{x} \in \mathcal{M}(\mathbf{z})} \frac{p_{0,x}(\mathbf{x})}{p_{0,x}(\mathbf{z})} d\mathbf{x} = \frac{1}{p_{0,x}(\mathbf{z})} \int_{\mathbf{x} \in \mathcal{M}(\mathbf{z})} p_{0,x}(\mathbf{x}) d\mathbf{x}. \quad (8)$$

The denominator of (8) is independent of  $\mathbf{x}$  on the manifold (6), and we have the identity

$$\int_{\mathbf{x} \in \mathcal{M}(\mathbf{z})} p_{0,x}(\mathbf{x}) d\mathbf{x} = p_{0,x}(\mathbf{z}).$$

Therefore,  $p_m(\mathbf{x}|\mathbf{z})$  integrates to 1 on the manifold.

### C. Sampling a PBN

We now summarize the stochastic sampling of a multi-layer PBN. We assume that the last layer of the network does not use an activation function (for theoretical purposes we can ignore the activation functions because they are assumed to be SMI and can be inverted). Let the network output be denoted by  $\mathbf{z}$ . Sampling proceeds as follows starting at the last (output) layer:

- 1) Set the network layer counter to the last layer.
- 2) We start by drawing a sample  $\mathbf{z}$  from the network output feature distribution  $g(\mathbf{z})$ .
- 3) Draw a sample from the manifold distribution  $p_m(\mathbf{x}|\mathbf{z})$ , i.e. draw a sample from  $\mathcal{M}(\mathbf{z})$ , weighted by the prior  $p_{0,x}(\mathbf{x})$ . How this is done depends on the prior distribution  $p_{0,x}(\mathbf{x})$ , which is selected from Table I. For the Gaussian case, drawing from  $p_m(\mathbf{x}|\mathbf{z})$  is straightforward, but for all the other cases, it is necessary to find a starting solution, any member of  $\mathcal{M}(\mathbf{z})$ , then use a form of MCMC to draw a sample from set  $\mathcal{M}(\mathbf{z})$  weighted by prior  $p_{0,x}(\mathbf{x})$  [23]. As an initial solution, one can either use a linear programming solver, but a better starting point is the conditional mean  $\bar{\mathbf{x}}_z$  as given later in Section III-D. If no solution exists, sampling has failed, return to step 1.
- 4) If this current layer is the first network layer, then sampling is finished, and  $\mathbf{x}$  is a sample of the input data. If this is not the first layer, then consider  $\mathbf{x}$  to be the output  $\mathbf{y}$  of the previous layer's activation function. To proceed, work backward by inverting the activation function and bias of the previous layer to obtain the previous layer's linear transformation output variable  $\mathbf{z}$ . Set layer counter to the previous layer, and proceed with step 3.

### D. Asymptotic Form of PBN

As elegant as (7) may be, it is difficult to work with. For example, integrating  $p_m(\mathbf{x}|\mathbf{z})$  to get the conditional mean,

$$\bar{\mathbf{x}}_z = \mathbb{E}_{\mathbf{x}|\mathbf{z}} = \int_{\mathbf{x} \in \mathcal{M}(\mathbf{z})} \mathbf{x} p_m(\mathbf{x}|\mathbf{z}) d\mathbf{x} \quad (9)$$

only has a closed form in case of a Gaussian prior. This is a result of the fact that the denominator  $p_{0,x}(\mathbf{z})$  is otherwise intractable.

Luckily, an “almost exact” approximation to  $p_{0,x}(\mathbf{z})$  can be found, resulting in a simple functional form for  $p_m(\mathbf{x}|\mathbf{z})$  for which the conditional mean can be found in closed form. Steven Kay [38] noted that in cases like this (linear combinations of non-Gaussian random variables), the moment generating function (MGF) of  $p_{0,x}(\mathbf{z})$  is in fact known exactly, and can be inverted to find  $p_{0,x}(\mathbf{z})$  using the saddle point approximation (SPA). The word “approximation” here is misleading because the inversion of the MGF, is “almost” exact. Although it is only a first-order approximation, the SPA integral has two important advantages: the integrand is known exactly, and the integral is carried out at the saddle point. As  $N$  becomes large, the integrand, as a result of the central limit theorem, takes an approximately Gaussian shape at the saddle point, which is exploited by the SPA to result in a solution for  $p_{0,x}(\mathbf{z})$  that is exact for all practical purposes.

Note that ideally,  $p_m(\mathbf{x}|\mathbf{z})$  has support only on  $\mathcal{M}(\mathbf{z})$ , but the “almost exact” functional form for  $p_m(\mathbf{x}|\mathbf{z})$ , called the *surrogate density* [36], [26], is a proper distribution in its own right, with support in all of  $\mathbb{X}$ . However, as  $N$  becomes large, the probability mass of the surrogate density converges around the manifold  $\mathcal{M}(\mathbf{z})$  (see Section VII-A in [23]) and the resulting closed-form expression for  $\bar{\mathbf{x}}_z$  converges quickly to the true value [29].

The surrogate density as well as the prior  $p_{0,x}(\mathbf{x})$  for all cases of  $\mathbb{X}$  in Table I can be represented by a single exponential-form density as follows

$$p_s(\mathbf{x}; \boldsymbol{\alpha}, \alpha_0, \beta) = \prod_{i=1}^N p_e(x_i; \alpha_i, \alpha_0, \beta), \quad (10)$$

where  $p_e(x; \alpha, \alpha_0, \beta)$  is a univariate distribution of the exponential class

$$\log p_e(x; \alpha, \alpha_0, \beta) = (\alpha_0 + \alpha)x + \beta x^2 + \log Z(\alpha, \alpha_0, \beta), \quad (11)$$

where  $\boldsymbol{\alpha} = \{\alpha_1, \dots, \alpha_M\}$ , and  $\log Z(\alpha, \alpha_0, \beta)$  is the normalization factor necessary such that  $p_e(x; \alpha, \alpha_0, \beta)$  integrates to 1. We also define the corresponding theoretical activation function using the expected value of  $p_e(x; \alpha, \alpha_0, \beta)$

$$\lambda(\alpha, \alpha_0, \beta) = \int_{\mathbb{X}} x p_e(x; \alpha, \alpha_0, \beta) dx.$$

In Table II, we provide  $p_e(x; \alpha, \alpha_0, \beta)$  for various choices of  $\mathbb{X}$ ,  $\alpha_0$ , and  $\beta$ . The prior is obtained for  $\boldsymbol{\alpha} = \mathbf{0}$

$$p_{0,x}(\mathbf{x}) = p_e(x; \mathbf{0}, \alpha_0, \beta).$$

TABLE II  
EXTENSION OF TABLE I SHOWING  $\alpha_0$ ,  $\beta$ , AND  $p_e(x; \alpha, \alpha_0, \beta)$  FOR ALL CASES.

$\mathbb{X}$	$\alpha_0$	$\beta$	$p_e(x; \alpha, \alpha_0, \beta)$	Name
$\mathbb{R}^N$	0	-5	$\mathcal{N}(x - \alpha)$	Gaussian.
$\mathbb{P}^N$	0	-5	$2\mathcal{N}(x - \alpha)$	Trunc. Gauss. (TG)
$\mathbb{P}^N$	-5	0	$\frac{(1-2\alpha)}{2} e^{-\frac{(1-2\alpha)}{2}x}$	Expon.
$\mathbb{U}^N$	0	0	$\left(\frac{\alpha}{e^{\alpha}-1}\right) e^{\alpha x}$	Trunc. Expon. (TED)

By comparing Tables I and II, it can be seen that the MaxEnt priors and activation functions given in Table I are special

cases of  $p_s(\mathbf{x}; \boldsymbol{\alpha}, \alpha_0, \beta)$  where  $\boldsymbol{\alpha} = \mathbf{0}$ , and the activation functions are the expected value as a function of  $\alpha$ . More precisely,

$$p_{0,x}(\mathbf{x}) = p_s(\mathbf{x}; \mathbf{0}, \alpha_0, \beta), \quad (12)$$

$$\lambda(\alpha) = \int_{\mathbb{X}} x p_e(x; \alpha, \alpha_0, \beta) dx, \quad (13)$$

where  $\alpha_0$  and  $\beta$  are provided in Table II.

We restate the following theorem, first published in [26]:

*Theorem 1:* Let prior  $p_{0,x}(\mathbf{x})$  be written as (12), having mean  $\lambda(\mathbf{0})$  as given in (13). Then, the surrogate density for  $p_m(\mathbf{x}|\mathbf{z})$  in (7) is  $p_s(\mathbf{x}; \mathbf{W}\mathbf{h}_z, \alpha_0, \beta)$ , where  $\mathbf{h}_z$  is value of  $\mathbf{h}$  that solves

$$\mathbf{W}'\lambda(\mathbf{W}\mathbf{h}) = \mathbf{z}. \quad (14)$$

Then, as  $N$  becomes large,  $p_s(\mathbf{x}; \mathbf{W}\mathbf{h}_z, \alpha_0, \beta) \rightarrow p_m(\mathbf{x}|\mathbf{z})$ .

Furthermore, the mean of the surrogate density is asymptotically (for large  $N$ ) equal to the mean of  $p_m(\mathbf{x}|\mathbf{z})$  and is given by

$$\bar{\mathbf{x}}_z = \lambda(\mathbf{W}\mathbf{h}_z). \quad (15)$$

For an outline of the proof, see [26].

In summary, the surrogate density converges to the posterior  $p_m(\mathbf{x}|\mathbf{z})$ , and so the mean of the surrogate density approaches the mean of  $p_m(\mathbf{x}|\mathbf{z})$ . This convergence occurs quickly as a function of  $N$ , as has been demonstrated in certain cases (see Fig. 8 in [23]). It has been shown that the error of the likelihood calculations when doing this are negligible [36], [29]. The surrogate density mean  $\bar{\mathbf{x}}_z$  given by (15) enjoys numerous properties. As conditional mean estimator, it has many well-known optimal properties [39]. Another special case of (15) corresponds to autoregressive spectral estimation, which can be generalized for any linear function of the spectrum, such as MaxEnt inversion of MEL band features [23]. A special case of (15) is mathematically the same as classical maximum entropy image reconstruction [40], [41]. It can also be shown that  $\mathbf{h}_z$  is the maximum likelihood estimate of  $\mathbf{h}$  under the likelihood function  $p(\mathbf{x}; \mathbf{h}) = p_s(\mathbf{x}; \mathbf{W}\mathbf{h}, \alpha_0, \beta)$  [42].

As we have noted, the surrogate density has a close relationship to  $p_{0,x}(\mathbf{z})$ , with  $\mathbf{h}_z$  being the saddlepoint for the SPA of  $p_{0,x}(\mathbf{z})$ . This follows from the fact that (14) is equivalent to the *saddle point equation* for the distribution of the linear sum of independent random variables (i.e. see [38], equation 25 in [38], on page 2245).

### E. Asymptotic Network and Deterministic PBN

The surrogate density can be seen as a layer in a generative network taking a familiar form. We first simplify notation by defining the function  $\gamma(\mathbf{h}) = \mathbf{W}'\lambda(\mathbf{W}\mathbf{h})$ . By definition,  $\gamma(\mathbf{h}_z) = \mathbf{z}$ . We also define the inverse:  $\mathbf{h}_z = \gamma^{-1}(\mathbf{z})$ . The concept of  $\gamma^{-1}(\mathbf{z})$  is illustrated in Figure 1 in which a two-layer network is shown. On the top of the figure is the forward path, and on the bottom is the reconstruction path that uses the asymptotic form of the network. We concentrate on just the first layer by using the shortcut path “(layer bypass)”. Feature  $\mathbf{z}$  is converted to  $\mathbf{h}_z$  through  $\gamma^{-1}(\mathbf{z})$ , then multiplied by  $\mathbf{W}$  to raise the dimension back to  $N$ , and finally passed





as a second step using Bayes rule:  $P(i|\mathbf{x}) = \frac{p(\mathbf{x}|i) P(i)}{p(\mathbf{x})}$ , however the normalizing factor  $p(\mathbf{x})$  is unnecessary if classification is implemented using

$$\arg \max_i \{p(\mathbf{x}|i) P(i)\}.$$

Decision boundaries are formed by the comparison of likelihood function values. To implement this with a PBN, we train a separate PBN on the training data for each class to obtain  $p(\mathbf{x}|i)$ . The advantage of training a separate model on each class is the large class-selectivity that it can provide. By training on each class separately, network weights become more fine-tuned to a given class. In convolutional layers, convolutional kernels take on patterns that act as basis functions for representing data of the given class. This approach, however, has one very important disadvantage: training a separate model on each class allows differences in initialization and training to greatly influence the resulting models and cause imbalances, which shift the decision boundaries, causing classification errors. There are ways to mitigate this. For example in speaker recognition, GMM-UBM [46] uses a single Gaussian mixture model (GMM) probability density estimate as a base model (the universal background model - UBM) which is then modified for each data class using just 1 step of the E-M algorithm. This eliminates the effects of randomly initializing each model. The general idea can be used when training PBNs. Class-dependent PBNs can be trained starting with a common model trained on all classes, but the benefits of this are limited and it can reduce class selectivity.

- 3) **Joint distribution (generative).** The joint-distribution approach trains a single model on the joint distribution of the class and label,  $p(\mathbf{x}, \mathbf{y})$ , then classifies using

$$\arg \max_i \{p(\mathbf{x}, \mathbf{y}_i)\}.$$

Although it avoids the model mismatch problem of the conditional distributions approach, it has one important flaw. Generative models are only approximations to the true distribution. In any approximation, compromises are made between conflicting goals: model simplicity and model accuracy. Since we intend to use joint distribution  $p(\mathbf{x}, \mathbf{y})$  as a classifier, and there usually is insufficient data to accurately estimate the true distribution, we must compromise by using a simplified model. We hope that the compromise favors high class selectivity, but we cannot guarantee this, nor can it be forced. In short, the joint-distribution approach avoids the disadvantages of the conditional distributions approach, but does not have its advantages, nor does it have the advantages of the discriminative approach.

Furthermore, a problem also arises because  $\mathbf{x}$  and  $\mathbf{y}$  have different forms, so the complete input data  $\{\mathbf{x}, \mathbf{y}\}$  is non-homogeneous. This is especially true when  $\mathbf{x}$  is multi-dimensional (i.e. an image or spectrogram). It is not clear how to insert  $\mathbf{y}$  into the input image, or combine it with the image so that it can be meaningfully processed by

a convolutional network. This problem can be avoided by injecting the label signal  $\mathbf{y}$  into intermediate convolutional layers after some down-sampling, or into dense (fully-connected) layers near the end of the network. Examples of injecting labels into the data can be found in design of class-dependent GANs [47] or in a deep belief network (DBN) [10].

The joint distribution approach has a further disadvantage when using PBNs. In a PBN, a kind of vanishing-gradients problem arises with respect to the labels. The higher the dimension a layer's input data has, the greater the effect of changing the layer weights has on the cost function. Therefore, the labels will have less effect if they interact with weights at the network output. As an aside, injecting label information in a PBN at multiple layers is not justified theoretically because the likelihood function for such a network may be intractable. In short, the joint distribution approach is problematic for PBN and likely to suffer from poor class-selectivity in the likelihood function.

To summarize, we prefer the conditional distributions approach for a PBN classifier because it has the potential for high class selectivity as a result of training networks individually on each class. But, we must seek ways to avoid the problem of model imbalance and the resulting shift of decision boundaries. This problem is solved by discriminative alignment.

#### IV. DISCRIMINATIVE ALIGNMENT OF PBN (PBN-DA)

For reasons mentioned in Section III-G, it is generally assumed that the discriminative approach to classification is superior to the generative approach. In short, estimating the class-dependent data distributions at high dimension is much harder than predicting the class label [2], [1]. But, because a PBN is a two-directional network one should be able to implement both paradigms in one network. But how? There appears to be a contradiction: discriminative classifiers are trained simultaneously on all data classes, but the conditional distributions approach, which we have said we want to use (see Section III-G), requires training separate networks on each class. A solution to this dilemma was proposed by the method of discriminative alignment [29], [27], [48] in which each class-dependent network is trained simultaneously as a generative model for the given class, but also as a discriminative model against "all other classes". This approach tends to "align" the network weights, giving the generative model high selectivity against the other classes, thus getting the best of both the generative and discriminative approaches. By causing high selectivity against other classes, it mitigates the problem of model mismatch because with high selectivity (i.e. high likelihood function slope when moving in the direction of other classes), so the decision boundaries will not shift much due to model mismatch.

To see this visually, we trained a simple PBN network on two-dimensional data with two data classes. In Figure 2, on the top row, we see data from the two classes (left), an intensity plot of the PBN likelihood function after training on the first data class (center), and the corresponding likelihood contours



(right). As we would expect, the likelihood has a peak at the location of the data. On the second row, the analogous plots are seen for a network trained on the second data class. However, as can be seen by the contour plots, there is not much selectivity against the other data class because the slope is highest in the orthogonal direction. In short, the class-selectivity appears to be poor.

We then re-trained the two PBNs with combined cost function. A classifier (cross-entropy) cost component was added to the PBN log-likelihood cost, giving the network the additional task of discriminating the two classes. In rows 3 and 4 of the figure, we see the results. Interestingly, now the contour plots show high selectivity against the other data class (i.e. high slope in the direction that separates the two data classes). The contours have been “discriminatively aligned”. Now, when classifying class 1 vs. class 2 using a straight Bayesian likelihood classifier, the classification results will resemble the properties of the discriminative classifier. In short, the best qualities of both network types are realized. The method has shown very promising results when compared to state of the art discriminative classifiers [29], [27], [48].

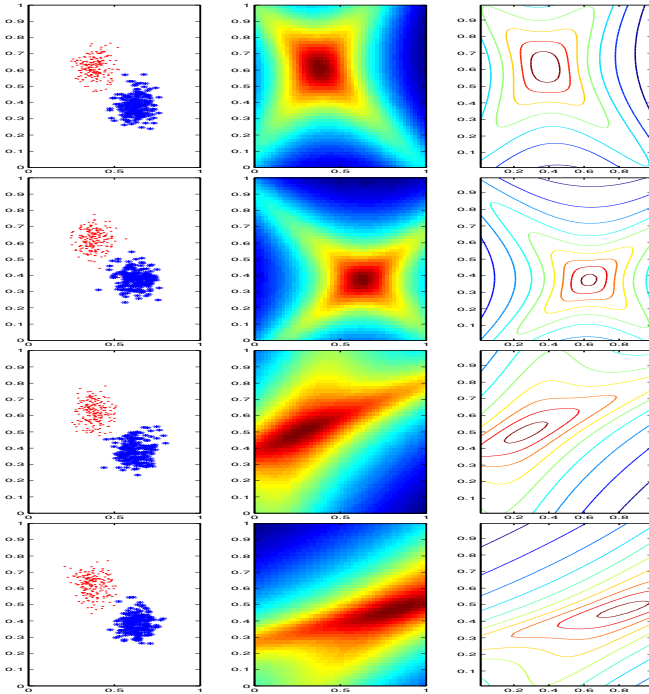


Fig. 2. From top to bottom: PBN trained on class 1 (red), PBN trained on class 2 (blue), PBN trained on class 1 with discriminative alignment, PBN trained on class 2 with discriminative alignment. Left column: input data, center: likelihood surface, right: contour lines of likelihood surface.

#### A. Self-Combination of PBN-DA

As we have claimed, the PBN is a two-directional network, incorporating two distinct network topologies in a single embodiment. In an  $K$ -class classifier scenario, the PBN-DA consists of  $K$  distinct networks, each trained on a single class. The forward networks are trained as a classifier to discriminate one class from all others, and the generative PBN

likelihood function is maximized over the training data of the same class. It follows, that one could use two methods to construct a classifier from a trained PBN-DA (a) a straight generative “conditional distributions” approach classifier based on comparing the projected log-likelihood functions of the  $K$  PBNs, and (b) a forward classifier based on finding the maximum output statistic across all class assumptions and all networks. We could therefore construct two distinct classifiers from a single set of trained PBNs.

Alternatively, the discriminative influence can be integrated into and combined with the generative classifier using a special output distribution. Notice that the last term in the projected likelihood function for each PBN is the output feature distribution, for example  $g(\mathbf{z})$  in (3). Let  $g_m(\mathbf{y})$  be the output feature distribution for the network trained on class  $m$ . Since  $g_m(\mathbf{y})$  is given, it can be constructed as an indicator function for class  $m$ , so that it has a higher likelihood if  $\mathbf{y}$  equals the label signal for class  $m$  (e.g. one-hot encoding), given by  $\mathbf{y}_m$ . For example,

$$g_m(\mathbf{y}) = \delta[\mathbf{y} - \mathbf{y}_m]. \quad (16)$$

In the experiments, we approximated (16) with a TED output activation function (See Table I) which, similar to sigmoid, has an output in the range  $[0, 1]$ . We assume the TED distribution

$$g_m(\mathbf{y}) = \prod_{i=1}^K \left( \frac{\alpha_{i,m}}{e^{\alpha_{i,m}} - 1} \right) e^{\alpha_{i,m} y_i},$$

where  $\mathbf{y} = \{y_1 \dots y_K\}$ , and  $\alpha_{i,m} = \{-C, i \neq m, +C, i = m\}$ . As can easily be verified,  $g_m(\mathbf{y})$  will have high value when  $\mathbf{y}$  is the one-hot encoding for class  $m$ , and a low value otherwise. The constant  $C$  can be used to control the relative importance of the output statistic (i.e. the class labels) in the projected LF. This has an effect similar to linear combining (ensembling) two classifier statistics (in one network!), and it is possible to experimentally determine the optimal value of  $C$ .

#### B. PBN-DA-HMM

The hidden Markov model (HMM) [49] was for a long time the state of the art in acoustic event classification and modeling. The HMM owes its success to two things:

- 1) The Markov assumption, which allows modeling events with unknown start time, and duration. The HMM is very forgiving against time-distorted or intermittent time sequences, a common problem in real-world speech and acoustic events.
- 2) The efficient forward algorithm for implementation of training and evaluation.

With the advent of convolutional neural networks (CNNs), the detection and modeling of events with unknown temporal location and size was greatly improved.

Despite the success of CNNs, it remains a possibility that the HMM is still useful as a component of a PBN. The LF of a PBN is formed recursively from the contributions of each layer according to the approach in equation (3). Suppose a PBN is broken into two parts. Let the hidden variables

coming out of the first half be denoted by  $\mathbf{h}$ . Then, using PDF projection, the second half of the network implements a PDF estimate  $\hat{\mathbf{h}}$ , denoted by  $G(\mathbf{h})$ , e.g. equation (3). However, it can be that the dimension of  $\mathbf{h}$  is small enough that one can use well-known PDF estimation methods, such as HMM, to replace, and possibly improve upon  $G(\mathbf{h})$ . The Markovian assumption exploited by the HMM, while over-simplified, provides an excellent compromise between tractability and generative modeling accuracy. There are two advantages to this, (a) the use of discriminative alignment in the pre-training of the first part of the network lends discriminative information to the features (class-selectivity), and (b) the use of HMM to replace the second part of the network has the stated advantages of the Markov model.

To summarize the method of PBN-DA-HMM: we train a full PBN as PBN-DA on class  $m$ , then when finished, shorten the network, tapping off the intermediate features  $\mathbf{h}_m$ , and estimate the distribution  $p_m(\mathbf{h}_m)$  using HMM. This is repeated for all classes  $m$ , and finally a class-specific classifier is constructed using the method in Section II-D.

## V. EXPERIMENT 1: ESC50 DATA SET

### A. Data Selection, Feature Selection, and Feature Extraction

The environmental sound classification data set (ESC50) [50] consists of 50 data classes, with 40 ten-second air-acoustic recordings in each data class. The classes are diverse, and it is difficult to represent them well by one feature extraction approach alone. As outlined in Section II, PDF projection allows the use of multiple feature extraction approaches in a single common generative model.

To this end, we attempted to match each data class with a feature set. This was done by segmenting the time-series into overlapped Hanning-weighted segments, then extracting log-MEL-band features. Time-series were then re-synthesized by reconstructing the power spectrum from the log-MEL-band features using maximum-entropy feature inversion [23], [26], as implemented by  $\bar{\mathbf{x}}_z$  in Section III-D, then reconstructing the complex-valued FFT using random-phase, reconstructing the segment time-series by inverse-FFT, Hanning-weighting and finally re-synthesizing time-series by using overlap-add. The time-series were played back and compared acoustically with the original. For almost all classes, a segment size and number of MEL bands could be found to result in very good reconstruction, as determined subjectively by ear. A large number of classes (23 classes) were well adapted to a segment size of 768, 2/3 overlap, and 48 log-MEL-spaced bands. The 23 classes (classes are numbered 0-49) were 0,1,6,9,10,11,13,16-19,21,23-25,27-30,36,45,47,49. The features for each 10-second event consisted of 624 time samples, resulting in a  $624 \times 48$  (time  $\times$  freq) matrix.

As explained in Section II-D, PBN classifiers can be constructed using multiple feature sets. But, this would require significantly more time and processing resources and would detract from evaluating the benefits of discriminative alignment together with HMM. Therefore, it was decided to put off any multiple-feature-set experiments using all 50 classes to future work and conduct a limited feasibility experiment on the 23-class subset using one feature type.

TABLE III  
MODIFIED RESNET ARCHITECTURE OF THE CNN.

layer name	structure	output size
input	BN (temporal axis)	$624 \times 48$
2D convolution	$7 \times 7$ , stride= (2, 1)	$312 \times 48 \times 16$
residual block	$\begin{pmatrix} 3 \times 3 \\ 3 \times 3 \end{pmatrix} \times 2$ , stride= 1	$155 \times 46 \times 16$
residual block	$\begin{pmatrix} 3 \times 3 \\ 3 \times 3 \end{pmatrix} \times 2$ , stride= 1	$78 \times 23 \times 32$
residual block	$\begin{pmatrix} 3 \times 3 \\ 3 \times 3 \end{pmatrix} \times 2$ , stride= 1	$39 \times 12 \times 64$
residual block	$\begin{pmatrix} 3 \times 3 \\ 3 \times 3 \end{pmatrix} \times 2$ , stride= 1	$20 \times 6 \times 128$
max pooling	$20 \times 1$ , stride= 1	$1 \times 6 \times 128$
flatten	BN	786
dense (embedding)	linear	128
sub-cluster AdaCos	4 sub-clusters per class	23

In a previous publication [48], we reported the results of experiments for an 8-class subset of these same 23 classes. We now provide results for all 23 classes. There were then  $23 \times 40 = 920$  total events.

To partition the data, we used 4:1 random data holdout, selecting 10 testing samples of the 40 samples of each class at random, and trained on the remaining 30. We did this four times, independently. There were 230 testing samples in each fold. The partitions were designated by letters A-D. For reproducibility, we provide these features and data folds online [51].

### B. Network Architectures

We used two network architectures in the experiments, (a) the “PBN networks”, which were trained separately on each of the 23 classes, and (b) a state of the art “CNN classifier” trained jointly as a classifier on all classes.

**PBN networks.** We used a network similar to that used in [48]. The eight-layer PBN network had three convolutional and 5 dense layers, ending with a classifier layer of 23 neurons. The input data is  $624 \times 48$  (time  $\times$  freq). Kernels in the three convolutional layers were  $8 \times 16$  kernels,  $30 \times 5$  kernels, and  $120 \times 3$  kernels respectively. Downsampling was  $3 \times 4$ ,  $3 \times 2$ , and  $3 \times 1$ . Convolutional border modes were “valid”. The dense layers had 512, 256, 128, 128, and 23 neurons. The last layer is the cross-entropy classifier (output) layer. The output of the third convolutional layer has dimension  $16 \times 120$ , which is tapped off for HMM processing. For the HMM, the data is seen as having 16 time steps and a feature dimension of 120. The twenty-three class-dependent PBN networks used linear activation at the output of the first 3 layers, in order to form a Gaussian group [27], and thereby greatly reducing the required computation. The remaining layers used the truncated Gaussian (TG) activation [52], similar in behavior to softplus, not unlike leaky Relu [53], but continuous (see Table I).

**CNN classifier.** The CNN model consists of a modified ResNet architecture [54] with about 800 k trainable parameters and is shown in Tab. III. It consists of an initial temporal mean

normalization operation, followed by a convolutional layer, 4 residual blocks, a temporal max-pooling operation and a dense layer with a linear activation function. The residual blocks each consist of two convolutional layers with kernels of size  $3 \times 3$ , batch normalization, a max pooling operation of size  $2 \times 2$  and use the ReLU activation function. Furthermore, the whole network does not contain any bias terms. The same architecture has been used successfully for the 8-class subset of ESC-50 [48], few-shot open-set acoustic event classification [55] and anomalous sound detection [56]. The model learns to embed audio data onto a hypersphere of fixed dimension and is trained by minimizing the angular margin loss sub-cluster AdaCos [57]. This loss is an angular margin loss with an adaptive scale parameter similar to AdaCos [58] but uses multiple instead of a single centers for each class, called sub-clusters. In this work, we used an embedding dimension of 128 and 4 randomly initialized sub-clusters for each class that are not adapted during training. When training the model, dropout with a probability of 50% is applied to the hidden representations before the last dense layer [59]. Additionally, two data augmentation techniques were used to improve the performance of the CNN. As a first technique, mixup [60] was applied to the input samples and their corresponding classes using a mixing coefficient sampled from a uniform distribution. Secondly, we applied random shifts up to 10% of the temporal dimension of the input representations (which was 640 time steps, so shifts were  $\pm 64$  samples). The CNN is trained for 500 epochs with a batch size of 8 using adam [61] and is implemented in Tensorflow [62]. To have a fair comparison, no external data was used to train the CNN.

After training, each test sample is embedded into the embedding space by applying the mapping learned by the CNN and projected to the unit sphere by normalizing with respect to the Euclidean norm. Then, similarity scores for each class are computed by taking the cosine similarity to the class-wise mean embeddings of all normalized embeddings extracted from the training samples. The class of the mean embedding with the shortest distance is used as the classification result.

### C. Network Training and Initialization

A separate PBN was trained on each of the 23 classes using discriminative alignment. About 1500 epochs were required. In addition to looking for convergence of the PBN LF, we also sought to have zero training errors in the discriminative task of “class  $m$ ” against “all other classes”. The cross-entropy discriminative cost function was scaled by 1000 before subtracting from the LF.

These networks were then used as-is for PBN-DA, then shortened and used for PBN-DA-HMM as described in Section IV-B. The networks were shortened by tapping off the output of the third layer, with data shape  $16 \times 120$ . We trained an HMM to estimate the probability distribution  $p_m(\mathbf{h}_m)$  of this output map. We then added  $\log p_m(\mathbf{h}_m)$  to the combined log-J-function for the first 3 layers to obtain the projected input data LF for PBN-DA-HMM.

For data augmentation during training, we used random circularly-indexed time shifts with a maximum of  $\pm 40$  time

segments. Because the CNN and HMM were significantly dependent on the random initialization, we always conducted three trials, and averaged the results. Due to computational expense, it was not practical to repeat the training of the PBN networks over multiple trials, but the four-fold partitioning provided adequate statistical diversity.

Note that the networks obtained by step (a) are used for PBN-DA in the experiments, and from step (d) for PBN-DA-HMM.

### D. Computational Requirements for PBNs

Using PBN Toolkit software [45], with a GPU (NVIDIA GeForce GTX 1050 Ti), and double precision (float64) with a batch size of 230, we are able to compute one epoch in 59 seconds. Double precision was needed to avoid problems during inversion of matrices. It typically required about 1500 epochs to train each of the 23 models, equating to about one day per class. With two computers, the training was finished in less than 2 weeks. We used stochastic gradient descent (or gradient ascent for LF), and ADAM optimization algorithm. Note that when training one model, we use data from all classes, not just the corresponding class. However, only data from the corresponding class is applied to the gradient of the LF cost function, whereas data from all classes is applied to the gradient of the discriminative cost function.

### E. Self-Combination of PBN-DA

We experimentally determined the optimal value of parameter  $C$ , as explained in Section IV-A, by evaluating the number of classification errors for PBN-DA, averaged over the four folds. As can be seen in Figure 3, there is a distinct

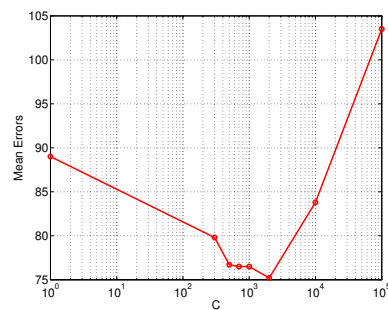


Fig. 3. Mean errors for self-combination as a function of  $C$ .

minimum at about  $C = 2000$ . The value  $C = 2000$  was used in subsequent experiments for PBN-DA.

### F. Individual Results

The number of errors out of a total of 230 events in each of the 4 data partitions are shown in Table IV for convolutional neural network (CNN), PBN-DA, and PBN-DA-HMM classifiers. Three random trials are shown for all methods except PBN-DA. Due to computational expense, the PBNs are trained just once. For PBN-DA-HMM, three independent trials pertain just to the HMM.



TABLE IV  
NUMBER OF ERRORS (OUT OF A TOTAL IF 230) ON EACH OF THE 4 DATA PARTITIONS FOR THE VARIOUS CLASSIFIERS.

Algorithm	Trial	Partition				mean
		A	B	C	D	
CNN	1	29	29	28	27	28.2
CNN	2	36	27	23	23	27.2
CNN	3	36	31	30	29	31.5
CNN	mean	33.7	29	27	26.3	<b>29</b>
PBN-DA	n/a	77	88	84	52	<b>75.25</b>
PBN-DA-HMM	1	20	21	17	59	29.3
PBN-DA-HMM	2	31	20	20	55	31.5
PBN-DA-HMM	3	30	18	7	54	27.3
PBN-DA-HMM	mean	27	19.7	14.7	56.0	<b>29.3</b>
CNN+PBN-DA	1	30	27	27	28	28
CNN+PBN-DA	2	27	26	24	24	25.2
CNN+PBN-DA	3	28	26	25	27	26.5
CNN+PBN-DA	mean	28.3	26.3	25.3	26.3	<b>26.6</b>
CNN+PBN-DA-HMM	1	18	13	14	15	15
CNN+PBN-DA-HMM	2	23	9	9	18	14.7
CNN+PBN-DA-HMM	3	19	11	10	17	14.2
CNN+PBN-DA-HMM	mean	20	11.0	11	16.7	<b>14.7</b>

First, it can be seen that the CNN classifier has significantly better performance than PBN-DA. In previous publications [29], [27], [48], PBN-DA competed more favorably with CNN, but it must be pointed out that in these experiments, CNN used more data augmentation during training (larger random data shifts - 64 vs. 40 and *mixup*).

Second, it can be seen that CNN has virtually identical performance as PBN-DA-HMM (29 versus 29.3 errors). This is remarkable, first because PBN-DA-HMM used less data augmentation than CNN, but more significantly, because PBN-DA-HMM is a generative conditional distributions classifier (See Section III-G). This is no doubt a result of the incorporation of both generative and discriminative approaches in a single network.

### G. Combined Results

It is well-known that combining the output of several classifiers usually improves the classification performance, especially if the combined classifiers (a) have comparable performance, and (b) they are based on different methods or views of the data. When looking at the individual performances in Table IV, it is clear that the stage is set for good classifier combination.

Classifier combination (ensembling) results are shown as a function of the linear combination factor for CNN with PBN-DA (in red) and CNN with PBN-DA-HMM (in blue) in Figure 4, and are summarized in Table IV. Some interesting things to note are that (a) PBN-DA-HMM works much better than PBN-DA, and combines also much better with CNN, (b) PBN-DA-HMM performs better than CNN in three of the four folds, and (c), that despite significantly worse performance in the last fold, the combination still works exceptionally well. This is an indication of the independence of the information being combined. It can also be seen in the figure that the linear combination factor at which the minimum number of errors is achieved is about the same for all four folds.

In Figure 5, the average of the four folds is seen, showing a factor of two reduction in classification errors at the best point. In Table IV, we summarize the classifier performance obtained by linear combination of CNN with PBN-DA and with PBN-DA-HMM, which is obtained at the optimal combining factor. This factor, about 6000, is held constant across the data folds<sup>2</sup>.

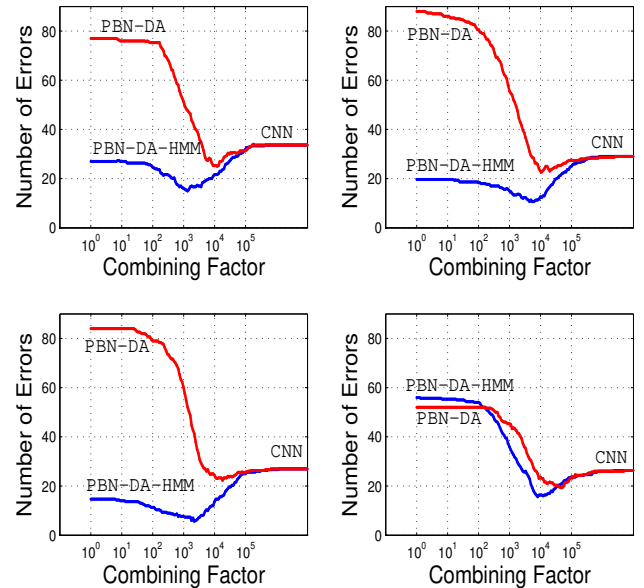


Fig. 4. Mean number of classification errors out of 230 samples, for each of the four partitions when combining PBN-DA-HMM with CNN.

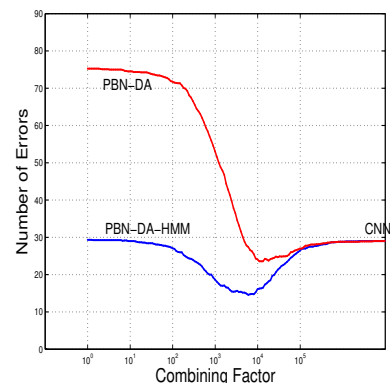


Fig. 5. Mean number of classification errors out of 230 samples, averaged over the four folds when combining PBN-DA-HMM with CNN.

### H. Reproducibility

Because we used a non-standard subset of ESC50 data, and non-standard data partitions, we make the feature data available, as well as software and instructions to reproduce the results in this paper as [45].

<sup>2</sup>The factor 6000 seems high, but this does not indicate anything about the relative importance of the two statistics. It is only due to the wide difference in the scale of the output statistics - log likelihood for PBN and cross-entropy classifier cost for CNN.

## VI. EXPERIMENT 2: ACOUSTIC TRENDS BLUE FIN DATA SET

### A. Data Description

The Australian Acoustic Trends Blue Fin data set [63] consists of acoustic recordings from various hydrophones, along with a set of annotations of marine mammal vocalizations that describe the bounding boxes of each vocalization (start and end time, as well as start and end frequency). We collected 200 examples of from each of six call types, denoted by “BM-Ant-A”, “BM-Ant-B”, “BM-Ant-Z”, “Bm.D”, “Bp-20Hz”, “Bp-Downsweep”. Example annotations are shown in Figure 6 from class “Bp-Downsweep”. An attempt was made to select only those annotations that were recognizable. The first of the three samples in the figure was deemed recognizable, and the last two were not and were discarded. In order to achieve 200 samples per event, it was necessary to relax the criteria somewhat. The data set is “dirty” in the sense that many examples are weak and occur simultaneously with interfering noise and interfering calls. A uniformly-sized time-window of 3072 samples at 250 Hz sample rate (12 seconds) was extracted for each selected annotation. For the

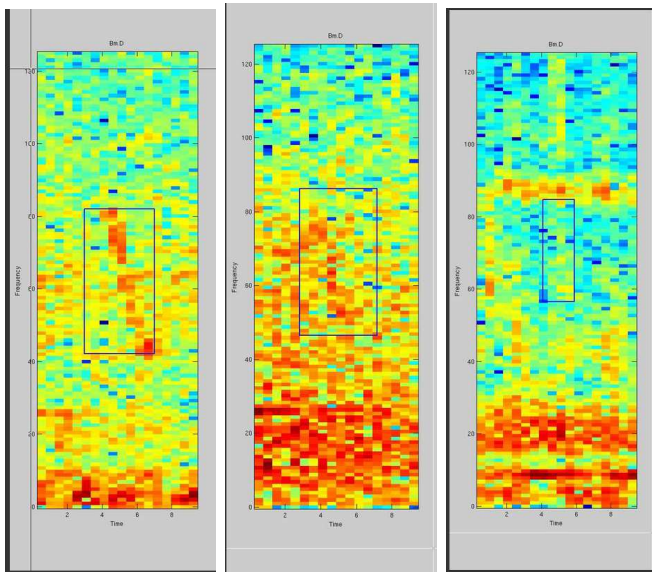


Fig. 6. Examples of annotations from Acoustic Trends Blue Fin Data Set of type “Bp-Downsweep”.

current experiments, the time-series were converted to log-band energy features with the following parameters: FFT size 384 with 128-sample shift (2/3 overlap), 40 linear-spaced hanning-weighted frequency bands, resulting in a  $40 \times 24$  feature map per event. Extracted .wav files and feature values for the selected annotations have been made available online [64].

### B. Networks

For the PBNs, a 5-layer network was used, consisting of two convolutional layers, followed by three dense layers of 128, 32, and 6 nodes. The first convolutional layer had  $8 \times 7 \times 13$  kernels with  $2 \times 4$  downsampling, resulting in 8 output

maps of  $12 \times 10$  (dimensions always given in time $\times$ freq). The second convolutional layer had  $48 \times 4 \times 10$  kernels with  $2 \times 1$  downsampling, resulting in 48 output maps of  $5 \times 1$  (dimensions always given in time $\times$ freq). Linear activation was used at the output of the convolutional layers, and truncated Gaussian (TG) activation function was used at the output of all dense layers (see Table I). One of the primary reasons for the high computational load of PBN is the need to invert matrices of dimension  $M \times M$ , where  $M$  is the total output dimension of a network layer. One of the means of mitigating this is to use linear activation functions in a few of the first network layers. These layers can then be grouped together in what is called a *Gaussian group* with a low output dimension [27]. We formed a Gaussian group from the first three layers.

For the benchmark CNN, the same network structure was used, but max-pooling was used instead of downsampling, and TG activation functions were used at the outputs of all layers.

### C. Training

Six separate PBNs were trained (one on each data class) using discriminative alignment and data augmentation of  $+/-3$  samples random circular time shifts and  $+/-1$  sample random frequency shift. Vernier shifts (i.e. not quantized to integer shifts) were accomplished by shifting the data in the frequency domain using 2D-FFT. The self-combination factor  $C = 3$  was used during training (see Section IV-A). For testing and evaluation, the value  $C = 300$  was used. The cross-entropy classifier cost (against “all other classes”) was multiplied by 2000 before being subtracted from the PBN log-likelihood value. A learning rate of  $2e^{-5}$  was used for 1500 epochs or until there were no more training errors (in the target class vs “all other classes” FFNN experiment).

For the benchmark CNN, we used drop-out regularization as well.

### D. PBN-DA-HMM

To implement PBN-DA-HMM, we tapped the output of the second convolutional layer, making a  $5 \times 48$  feature map, where the first dimension was time. The PDF of this feature was estimated using a 4-state HMM, where each state was represented by a Gaussian mixture (GMM) of 3 components. To prevent covariance collapse, a value of 0.12 was added to the diagonal elements of the GMM covariance matrices.

### E. Results

Results are shown for PBN-DA (in red) and PBN-DA-HMM (in blue) in combination with the benchmark CNN for all four data folds in Figure 7, and averaged over the folds in Figure 8. Shown is total errors out of a total of 300 for each data fold. These results are strikingly similar to the first experiment, using a completely different data set. As in the first experiment, PBN-DA performed well, but not as well as the benchmark CNN, and resulted in significant error reduction when combined with the CNN. Also, as in the first experiment, PBN-DA-HMM performed exceedingly well, better than the benchmark CNN, and resulted in a very significant 2:1 error reduction.

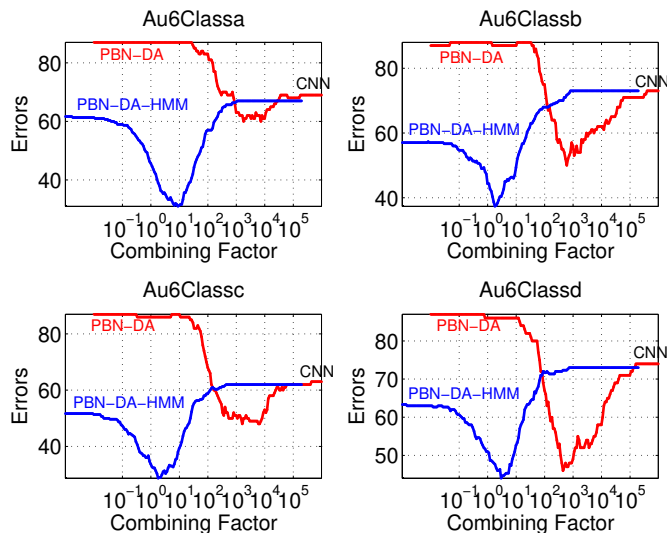


Fig. 7. Results of PBN-DA vs. PBN-DA-HMM in combination with CNN for Australian Blue Fin data. Shown is number of errors out of 300 for each of the four data folds.

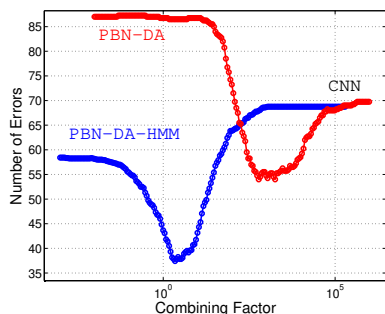


Fig. 8. Results of PBN-DA vs. PBN-DA-HMM in combination with CNN for Australian Blue Fin data. Shown is number of errors out of 300 averaged over the four data folds.

## VII. CONCLUSION AND FUTURE WORK

In this paper, generative classifiers called PBN-DA and PBN-DA-HMM have been described that combine both generative and discriminative methods in a single network. Generative PBN networks are trained separately on each class using discriminative alignment, ensuring that the generative models are selective against the other data classes. Optionally, when (a) the input data has a time dimension where convolutional layers can be applied, and (b) a suitable reduced-dimension latent variable is present at the output of an intermediate network layer, then the PBN-DA-HMM method can be applied. To do this, the PBNs are shortened, tapping off at the suitable intermediate layer. The probability density of these latent variables is estimated using HMMs, which leverage the Markov assumption to create good probability density estimates. When a time-dimension is not available, it should be possible to apply Gaussian mixture model effectively.

Two separate experiments using vastly different acoustic data sets, confirm that the approach does indeed attain some the best qualities of both discriminative and generative approaches. In fact, it is seen that the performance of PBN-DA-

HMM is virtually identical to or better than a state of the art CNN, and by linear combining with CNN attains a factor of two reduction in error rate. The relatively high computational burden of PBN means that the approach is suited to problems with high cost of errors, such as in military and human safety applications.

Software implementations of PBN and related programs [51], [45] and data sets for the current problems are made available online [64].

For future work, it is planned to extend the results to the full ESC50 data set.

## REFERENCES

- [1] I. Goodfellow, Y. Bengio, A. Courville, and Y. Bengio, *Deep Learning*. Cambridge, MA: MIT press, 2016.
- [2] V. Vapnik, *The Nature of Statistical Learning*. Springer, 1999.
- [3] Z. Zheng, X. Yang, Z. Yu, L. Zheng, Y. Yang, and J. Kautz, "Joint discriminative and generative learning for person re-identification," in *CVPR 2019, Long Beach, CA, June 2019*, pp. 2133–2142.
- [4] J. Gordon and J. M. Hernández-Lobato, "Combining deep generative and discriminative models for bayesian semi-supervised learning," *Pattern Recognition*, vol. 100, 2020.
- [5] Z. Tu, "Learning generative models via discriminative approaches," in *2007 IEEE Conference on Computer Vision and Pattern Recognition*, 2007, pp. 1–8.
- [6] R. Raina, Y. Shen, A. Y. Ng, and A. McCallum, "Classification with hybrid generative/discriminative models," in *NIPS 2003, Vancouver and Whistler British Columbia, Canada, December 2003*.
- [7] H. Liu and P. Abbeel, "Hybrid discriminative-generative training via contrastive learning," *ArXiv*, 2020. [Online]. Available: <https://doi.org/10.48550/arXiv.2007.09070>
- [8] T. Jaakkola and D. Haussler, "Exploiting generative models in discriminative classifiers," in *NIPS 1998, Denver, 1998*.
- [9] M. Schuster and K. Paliwal, "Bidirectional recurrent neural networks," *IEEE Transactions on Signal Processing*, vol. 45, no. 11, pp. 2673–2681, 1997.
- [10] G. E. Hinton, S. Osindero, and Y.-W. Teh, "A fast learning algorithm for deep belief nets," in *Neural Computation 2006*, 2006.
- [11] M. Welling, M. Rosen-Zvi, and G. Hinton, "Exponential family harmoniums with an application to information retrieval," *Advances in neural information processing systems*, 2004.
- [12] P. Li and P. Nguyen, "On random deep weight-tied autoencoders: Exact asymptotic analysis, phase transitions, and implications to training," *ICLR*, 2019.
- [13] S. Odaibo, "Tutorial: Deriving the standard variational autoencoder (vae) loss function," 2019.
- [14] C. Doersch, "Tutorial on variational autoencoders," 2021. [Online]. Available: <https://doi.org/10.48550/arXiv.1606.05908>
- [15] I. Higgins, L. Matthey, A. Pal, C. Burgess, X. Glorot, M. Botvinick, S. Mohamed, and A. Lerchner, "Learning basic visual concepts with a constrained variational framework," in *Proceedings of ICLR 2017*, 2017, pp. 595–597.
- [16] I. Kobyzev, S. J. D. Prince, and M. A. Brubaker, "Normalizing flows: An introduction and review of current methods," *IEEE Trans. Pattern Anal. Mach. Intell.*, vol. 43, no. 11, pp. 3964–3979, 2021.
- [17] D. Nielsen, P. Jaini, E. Hoogeboom, O. Winther, and M. Welling, "Survae flows: Surjections to bridge the gap between vases and flows," in *NIPS 2020 (Virtual)*, 2020.
- [18] P. M. Baggenstoss and F. Govaers, "A comparison of pdf projection with normalizing flows and survae," *arXiv*, 2023.
- [19] P. M. Baggenstoss, "The PDF projection theorem and the class-specific method," *IEEE Trans Signal Processing*, pp. 672–685, March 2003.
- [20] —, "Beyond moments: Extending the maximum entropy principle to feature distribution constraints," *Entropy*, vol. 20, no. 9, 2018. [Online]. Available: <http://www.mdpi.com/1099-4300/20/9/650>
- [21] —, "Maximum entropy PDF design using feature density constraints: Applications in signal processing," *IEEE Trans. Signal Processing*, vol. 63, no. 11, Jun. 2015.
- [22] P. M. Baggenstoss and S. Kay, "Nonlinear dimension reduction by pdf estimation," *IEEE Transactions on Signal Processing*, 2022.



- [23] P. M. Baggenstoss, "Uniform manifold sampling (UMS): Sampling the maximum entropy pdf," *IEEE Transactions on Signal Processing*, vol. 65, no. 9, pp. 2455–2470, May 2017.
- [24] —, "Class-specific model mixtures for the classification of time-series," 2014.
- [25] —, "Class-specific model mixtures for the classification of acoustic time-series," *IEEE Trans. AES*, Aug. 2016.
- [26] —, "A neural network based on first principles," in *ICASSP 2020, Barcelona (virtual)*, Barcelona, Spain, Sep 2020.
- [27] —, "Using the projected belief network at high dimensions," *Proceedings of EUSIPCO 2022, Belgrade*, 2022.
- [28] —, "Applications of projected belief networks (PBN)," *Proceedings of EUSIPCO, A Coruña, Spain*, 2019.
- [29] —, "Discriminative alignment of projected belief networks," *IEEE Signal Processing Letters*, Sep 2021.
- [30] —, "On the equivalence of hanning-weighted and overlapped analysis windows using different window sizes," *IEEE Signal Processing Letters*, vol. 19, no. 1, pp. 27–30, Jan 2012.
- [31] Z. Zhu, S. Kay, and R. S. Raghavan, "Information-theoretic optimal radar waveform design," *IEEE Signal Processing Letters*, vol. 24, no. 3, pp. 274–278, 2017.
- [32] J.-P. Nadal and N. Parga, "Nonlinear neurons in the low-noise limit: a factorial code maximizes information transfer," *Network: Computation in Neural Systems*, vol. 5, no. 4, pp. 565–581, 1994.
- [33] D. Lin and X. Tang, "Conditional infomax learning: an integrated framework for feature extraction and fusion," in *European conference on computer vision*. Springer, 2006, pp. 68–82.
- [34] G. Deco and D. Obradovic, *An Information-Theoretic Approach to Neural Computing*. Springer, 1996.
- [35] S. Kay, *Information-Theoretic Signal Processing and its Applications*. Sachuest Point Publishers, 2020.
- [36] P. M. Baggenstoss, "On the duality between belief networks and feed-forward neural networks," *IEEE Transactions on Neural Networks and Learning Systems*, pp. 1–11, 2018.
- [37] E. T. Jaynes, "Information theory and statistical mechanics i," *Physical Review*, p. 171–190, 1957.
- [38] S. M. Kay, A. H. Nuttall, and P. M. Baggenstoss, "Multidimensional probability density function approximations for detection, classification, and model order selection," *IEEE Transactions on Signal Processing*, vol. 49, no. 10, pp. 2240–2252, Oct 2001.
- [39] S. Kay, *Fundamentals of Statistical Signal Processing, Estimation Theory*. Prentice Hall, Upper Saddle River, New Jersey, USA, 1993.
- [40] S. J. Wernecke and L. R. D'Addario, "Maximum entropy image reconstruction," *IEEE Trans. Computers*, vol. C-26, no. 4, pp. 351–364, 1977.
- [41] G. Wei and H. Zhen-Ya, "A new algorithm for maximum entropy image reconstruction," in *Proceedings of ICASSP-87*, vol. 12, April 1987, pp. 595–597.
- [42] O. Barndorff-Nielsen and D. R. Cox, "Edgeworth and saddle-point approximations with statistical applications," *Journal of the Royal Statistical Society: Series B (Methodological)*, vol. 41, no. 3, pp. 279–299, 1979.
- [43] P. M. Baggenstoss, "Applications of projected belief networks (pbn)," in *Proceedings of EUSIPCO 2019, La Coruña, Spain*, Sep 2019.
- [44] —, "Improved auto-encoding using deterministic projected belief networks and compound activation functions," *Proceedings of EUSIPCO 2023, Helsinki*, 2023.
- [45] P. Baggenstoss, "PBN Toolkit," accessed: 2023-10-28. [Online]. Available: <http://class-specific.com/pbntk>
- [46] U. Bhattacharjee and K. Sarmah, "Gmm-ubm based speaker verification in multilingual environments," *IJCSI International Journal of Computer Science Issues*, vol. 9, no. 2, pp. 373–380, 2012.
- [47] T. Miyato and M. Koyama, "cGANs with projection discriminator," in *ICLR 2018*. IEEE, 2018.
- [48] P. M. Baggenstoss and K. Wilkinghoff, "Novel generative classifier for acoustic events (accepted)," *Proceedings of EUSIPCO 2023, Helsinki*, 2023.
- [49] L. R. Rabiner, "A tutorial on hidden Markov models and selected applications in speech recognition," *Proceedings of the IEEE*, vol. 77, no. 2, pp. 257–286, February 1989.
- [50] K. J. Piczak, "ESC: Dataset for Environmental Sound Classification," 2015. [Online]. Available: <https://doi.org/10.7910/DVN/YDEPUT>
- [51] P. Baggenstoss, "CSF Toolkit," accessed: 2021-10-28. [Online]. Available: <http://class-specific.com/csftk>
- [52] —, "New restricted Boltzmann machines and deep belief networks for audio classification," *2021 ITG Speech Communication, Kiel (Virtual)*, 2021.
- [53] A. L. Maas, A. Y. Hannun, and A. Y. Ng, "Rectifier nonlinearities improve neural network acoustic models," in *30th International Conference on Machine Learning (ICML)*, 2013.
- [54] K. He, X. Zhang, S. Ren, and J. Sun, "Deep residual learning for image recognition," in *Conference on Computer Vision and Pattern Recognition, CVPR*. IEEE, 2016, pp. 770–778.
- [55] K. Wilkinghoff and F. Fritz, "On using pre-trained embeddings for detecting anomalous sounds with limited training data," in *31st European Signal Processing Conference (EUSIPCO)*. IEEE, 2023.
- [56] K. Wilkinghoff, "Design choices for learning embeddings from auxiliary tasks for domain generalization in anomalous sound detection," in *International Conference on Acoustics, Speech and Signal Processing (ICASSP)*. IEEE, 2023.
- [57] —, "Sub-cluster AdaCos: Learning representations for anomalous sound detection," in *International Joint Conference on Neural Networks (IJCNN)*. IEEE, 2021.
- [58] X. Zhang, R. Zhao, Y. Qiao, X. Wang, and H. Li, "AdaCos: Adaptively scaling cosine logits for effectively learning deep face representations," in *Conference on Computer Vision and Pattern Recognition (CVPR)*. IEEE, 2019, pp. 10823–10832.
- [59] G. E. Hinton, N. Srivastava, A. Krizhevsky, I. Sutskever, and R. Salakhutdinov, "Improving neural networks by preventing co-adaptation of feature detectors," *CoRR*, vol. abs/1207.0580, 2012.
- [60] H. Zhang, M. Cisse, Y. N. Dauphin, and D. Lopez-Paz, "Mixup: Beyond empirical risk minimization," in *6th International Conference on Learning Representations (ICLR)*, 2018.
- [61] D. P. Kingma and J. Ba, "Adam: A method for stochastic optimization," in *3rd International Conference on Learning Representations (ICLR)*, 2015.
- [62] M. Abadi et al., "Tensorflow: A system for large-scale machine learning," in *12th USENIX Symposium on Operating Systems Design and Implementation (OSDI)*, 2016, pp. 265–283.
- [63] B. Miller, K. Stafford, I. Van Opzeeland, D. Harris, F. Samaran, A. Širović, S. Buchan, K. Findlay, N. Balcazar, S. Nieuwkirk, E. Leroy, M. Aulich, F. Shabangu, R. Dziak, W. Lee, and J. Hong, "An annotated library of underwater acoustic recordings for testing and training automated algorithms for detecting antarctic blue and fin whale sounds," in *Australian Antarctic Data Centre*, 2020. [Online]. Available: [https://data.aad.gov.au/metadata/records/AcousticTrends\\_BlueFinLibrary](https://data.aad.gov.au/metadata/records/AcousticTrends_BlueFinLibrary)
- [64] P. Baggenstoss, "Selected events from acoustic trends blue fin data set," accessed: 2023-10-28. [Online]. Available: <http://class-specific.com/au6>